DIGITAL ACCESS TO SCHOLARSHIP AT HARVARD

Cortical synaptogenesis and excitatory synapse number are determined via a Neuroligin-1-dependent intercellular competition

Citation	Kwon, Hyung-Bae, Yevgenia Kozorovitskiy, Won-Jong Oh, Rui T. Peixoto, Nazia Akhtar, Jessica L. Saulnier, Chenghua Gu, and Bernardo L. Sabatini. 2012. "Cortical synaptogenesis and excitatory synapse number are determined via a Neuroligin-1-dependent intercellular competition." Nature neuroscience 15 (12): 1667-1674. doi:10.1038/nn.3256. http://dx.doi.org/10.1038/nn.3256.
Published Version	doi:10.1038/nn.3256
Accessed	April 17, 2018 4:26:50 PM EDT
Citable Link	http://nrs.harvard.edu/urn-3:HUL.InstRepos:11708638
Terms of Use	This article was downloaded from Harvard University's DASH repository, and is made available under the terms and conditions applicable to Other Posted Material, as set forth at http://nrs.harvard.edu/urn-3:HUL.InstRepos:dash.current.terms-of-use#LAA

(Article begins on next page)

Cortical synaptogenesis and excitatory synapse number are determined via a Neuroligin-1-dependent intercellular competition

Hyung-Bae Kwon[1,3], **Yevgenia Kozorovitskiy**[1], **Won-Jong Oh**[2], **Rui T. Peixoto**[1], **Nazia Akhtar**[1], **Jessica L. Saulnier**[1], **Chenghua Gu**[2], and **Bernardo L. Sabatini**[1,4]

[1]Howard Hughes Medical Institute, Department of Neurobiology, Harvard Medical School, Boston, Massachusetts 02115

[2]Department of Neurobiology, Harvard Medical School, Boston, Massachusetts, USA

Abstract

Members of the neuroligin (NL) family of cell-adhesion proteins are found at excitatory and inhibitory synapses and are mutated in some familial forms of autism spectrum disorders. Although they display synaptogenic properties in heterologous systems, a function of NLs *in vivo* in regulating synapse formation and synapse number has been difficult to establish. Here we show that neuroligin-1 (NL1), which is located at excitatory post-synaptic densities, does regulate activity-dependent synaptogenesis as well as mature synapse number on cortical layer 2/3 pyramidal neurons *in vivo*. However, synapse number is not sensitive to absolute NL1 levels but rather to transcellular differences in the relative amounts of NL1. These effects are independent of the cell-autonomous regulation of NMDA-type glutamate receptors by absolute levels of NL1. Our data indicate that transcellular competitive processes govern synapse formation and number in developing cortex and that NL1 plays a central function in these processes.

Introduction

Neocortical development progresses through stages of synaptogenesis and synapse refinement that establish cell-to-cell connectivity and network topology[1, 2]. During early development, intrinsically-generated patterned activity helps establish the correct connectivity between and within brain regions[3, 4]. During later development, perturbations of sensory experience of the animal alter connectivity within sensory cortices, indicating that the activity-dependent control of synaptogenesis shapes post-natal development[5–7]. Additionally, molecular cues, including gradients of signaling molecules and intercellular cell-adhesion complexes, regulate many aspects of circuit and cellular development[8–11]. Thus, post-natal development of cerebral cortex is governed by activity-dependent and independent mechanisms that regulate synaptic connectivity.

Transsynaptic cell-adhesion molecules, which are present at synapses and mediate transcellular and intracellular signals, regulate both activity-dependent and independent synaptic maturation during development[9, 10, 12, 13]. The Neuroligin family of proteins (NLs), consisting of synaptically-localized cell-adhesion molecules that are expressed in a developmentally regulated manner, have been proposed to regulate many aspects of synaptic transmission and development[14, 15]. Four NLs have been identified in mice and localization

[4]Corresponding author: Bernardo L. Sabatini, Howard Hughes Medical Institute, Department of Neurobiology, Harvard Medical School, 220 Longwood Ave., Boston, MA 02115, bsabatini@hms.harvard.edu.
[3]Present address: Max Planck Florida Institute, Jupiter, Florida 33458, USA

of each family member varies[16–18]. For example, NL1 is predominantly postsynaptic at excitatory synapses[14] and binds to presynaptic neurexins, an interaction that is thought to act after initial synapse formation to regulate synapse maturation[19]. In contrast, NL2 is found predominantly at inhibitory synaptic terminals[15] and regulates assembly of GABAergic synapses[20]. The importance of NL-dependent signaling to human brain development is highlighted by the finding of mutations in NLs and neurexins in families with genetic forms of autism[21–23].

Defining the functions of NL1 in synapse development and separating its transcellular vs. cell-autonomous contributions have been difficult. Up- and down-regulation of NL1 increases and decreases, respectively, synaptic currents mediated by NMDA-type glutamate receptors (NMDARs) [19, 24–26] (but see[15]). However, whether the number and structure of excitatory synapses are regulated by NL1 is unclear, and results from studies of various preparations are in conflict. NL1 expressed in non-neuronal cells attracts axons and induces formation of rudimentary presynaptic boutons[27], suggesting that NL1 is intrinsically synaptogenic. In cultured neurons, the number of glutamatergic synapses increases with overexpression of NL1[19, 28–34] and decreases with knock-down of NL1 with RNA-interference[29]. On the other hand, despite a perinatal lethal phenotype and perturbations of synaptic transmission in respiratory nuclei, neurons from triple NL1-3 knockout (KO) mice have normal synapse number and synaptic ultrastructure[15]. Similarly, widespread or sparse loss of NL1 in hippocampus or amygdala does not alter synapse number[15, 24, 25]. Thus, studies of cultured neurons whose NL1 levels have been manipulated *ex vivo* indicate that NL1 regulates synapse number and spine morphology, whereas analyses *in vivo* or of tissue acutely prepared from KO animals have not supported this conclusion.

A possible explanation for these conflicting results is that differences in activity patterns between neurons in culture and *in vivo* may reveal or mask effects of NL1 loss, a hypothesis that is consistent with the dependence of the synaptic effects of NL1 overexpression on activity levels in cultured neurons[19]. Alternatively, differences may arise due to the timing of the manipulation, the brain region examined, or the fraction of neurons that are affected.

To determine if NL1 regulates the formation, morphology, and function of excitatory synapses *in vivo*, we examined cortical layer 2/3 pyramidal neurons whose levels of NL1 had been up- or down-regulated from the time of neuronal birth. Synapse structure and function in tissue in which all neurons lack NL1 was compared to that in genetically mosaic tissue in which NL1 levels vary from cell to cell. Analysis in acute brain slices revealed that early postnatal defects in NMDARs are triggered by both global and sparse loss of NL1. Conversely, NL1-dependent changes in synapse number and activity-dependent synaptogenesis are revealed only when differences in NL1 levels exist across neurons. For this reason, the effects of NL1 knock-down or overexpression are different in wild-type, NL1 heterozygote, and NL1 null mice. Thus, transcellular differences in NL1 levels during development, but not the absolute levels of NL1 in individual cells, regulate activity-dependent synaptogenesis and determine the mature structure and function of cortical neurons.

RESULTS

Modulation of excitatory synapse number by sparse knock-down of neuroligin-1

To determine if postsynaptic NL1 levels regulate synapse development *in vivo*, we induced RNA interference (RNAi) to knock-down NL1 in cortical neurons using *in utero* electroporation. Electroporation at embryonic stage 15.5, when progenitors for layer 2/3 cortical neurons are accessible, results in sparse transfection (up to ~20%) of layer 2/3

pyramidal neurons while allowing neurons to develop *in vivo* under largely normal network activity and connectivity (Fig. 1a).

Plasmids encoding small-hairpin RNAs (shRNA) with sequence homology to mouse NL1 were designed and purchased (see methods). Constructs were tested *in vitro* for knock-down of an NL1-EGFP fusion protein in HEK293 cells (Fig. 1b). The most effective construct, sh-NL1 #7, was used for the majority of subsequent experiments and is referred to as sh-NL1 below. This construct was effective in neurons, as transduction of dissociated cortical cultures with lentiviruses encoding the plasmid strongly reduced endogenous NL1 levels (Fig. 1c). Reduction of NL1 expression did not significantly alter levels of the family members NL2 and NL3 (Fig. 1d).

Examination of dendritic spines of sh-NL1 expressing neurons in acute slices prepared from postnatal day 17–21 *in utero* electroporated mice revealed that spine length and head area were increased and spine density was reduced compared to control EGFP transfected neurons (Supplementary Fig. 1a and Fig. 1e; sh-NL1 and control: 0.50±0.06, 0.91±0.04 spines/μm, 11–17 neurons, 25–27 dendrites, $p<0.05$). Cotransfection of sh-NL1 and human NL1 (hNL1), which contains sequence alterations in the region targeted by sh-NL1, suppressed the effects of NL1 knockdown (Supplementary Fig. 1a and Fig. 1e; 0.93±0.05 spines/μm, 10 neurons, 22 dendrites, $p>0.05$ vs. control), indicating that spine changes in sh-NL1-expressing neurons were due to loss of NL1. Similar morphological changes were observed in biolistically transfected hippocampal CA1 pyramidal neurons in organotypic slice cultures (Supplementary Fig. 2).

The frequency of miniature excitatory postsynaptic currents (mEPSCs) in NL1 knock-down neurons measured by whole-cell voltage-clamp was reduced without significant effect on their amplitude (Fig. 1g; sh-NL1 and control: amplitude: 7.40±0.54 pA, n=8, 8.36±0.41 pA, n=10, $p>0.05$; frequency: 0.82±0.12 Hz, n=8, 1.40±0.17 Hz, n=10, $p<0.05$). These effects were prevented by cotransfection hNL1 (Fig. 1g; amplitude: 8.71±0.42 pA, frequency: 1.81±0.20 Hz, n=10, $p>0.05$ vs. control), confirming the NL1-dependence of the effects on synapse number.

Nevertheless, similar effects were not observed in layer 2/3 pyramidal neurons of NL1 knock-out (KO) mice, which had no spine morphology or density changes compared to those in wildtype (WT) animals (Fig. 1f and Supplementary Fig. 1b; NL1$^{+/+}$: 0.91±0.1 spines/μm, 9 neurons/19 dendrites, NL1$^{-/-}$: 0.88±0.05 spines/μm, 10 neurons/22 dendrites, $p>0.05$). Importantly, introduction of sh-NL1 into NL1$^{-/-}$ neurons had no effect on the structure and density of spines (Supplementary Fig. 1b and Fig. 1g; NL1$^{-/-}$+ sh-NL1: 0.87±0.05 spines/μm, 10 neurons/19 dendrites, $p>0.05$ for each vs. NL1$^{+/+}$), confirming that the effects of sh-NL1 in WT animals were due to the loss of NL1 and not to possible off-target effects of the shRNA. Similarly, no changes in mEPSC amplitude and frequency were observed (Fig. 1h; NL1$^{+/+}$, NL1$^{-/-}$, and NL1$^{-/-}$+sh-NL1: frequency: 1.35±0.16 Hz, n=8, 1.28±0.13, n=9, 1.30±0.1, n=8; amplitude: 9.0±1.5 Hz, n=8, 8.8±1.7, n=9, 8.7±1.3, n=9). Thus reduction of NL1 levels in a sparse subset of cortical neurons alters synapse number whereas global knockout of the gene has no effect. Importantly, both sets of experiments were carried out in the same cell type and in the same *in vivo* context.

Neuroligin-1 modulates NMDAR-mediated currents and Ca^{2+} transients of individual postsynaptic terminals

A possible mechanism for NL1-dependent modulation of synapse number is by reduction of NMDARs, which regulate synapse structure and function via a variety of mechanisms and whose activation triggers activity-dependent synaptogenesis in developing layer 2/3 pyramidal neurons[35]. To determine if the functional properties of individual postsynaptic

terminals are differentially affected by sparse vs. global manipulations of NL1, we used glutamate uncaging to examine AMPAR- and NMDAR-mediated currents and Ca^{2+} influx. Whole-cell recordings were obtained from layer 2/3 pyramidal neurons using intracellular solutions containing Alexa Fluor-594 (20 μM) to visualize morphology and a Ca^{2+} indicator, Fluo-5F (300 μM), to monitor intracellular Ca^{2+}. MNI-glutamate (5 mM) in the extracellular solution was photolysed to release glutamate by 2-photon excitation with 0.5 ms-long 720 nm laser pulses. To improve voltage-clamp and monitor single terminal AMPAR and NMDAR signals, voltage-gated potassium, sodium, and Ca^{2+} channels were blocked with a cocktail of antagonists (see methods). Uncaging glutamate near a visualized spine elicited uncaging-evoked AMPAR- and NMDAR-EPSCs (AMPAR-uEPSCs and NMDAR-uEPSCs) that were measured by holding cells at −60 and +40 mV, respectively (Fig. 2b). Simultaneous measurement of green fluorescence was used to monitor Ca^{2+} transients in the active spine and neighboring dendrite (Fig. 2a,b) at −60 mV. Under these conditions Ca^{2+} enters the spine through NMDARs which are not fully blocked by extracellular Mg^{2+} [36, 37].

Voltage-clamp recordings from sh-NL1-transfected neurons did not reveal significant differences in AMPAR-uEPSCs compared to control (Fig. 2c,f; sh-NL1 and control: 14.0±1.6 pA, n=25; 14.2±1.7, n=20, p>0.05). However, at these same postsynaptic terminals NMDAR uEPSCs (sh-NL1 and control: 5.0±0.8 pA; n=25, 13.7±1.8 pA, n=20, p<0.05) and Ca^{2+} transients (sh-NL1 and control $\Delta G/G_{sat}$: 4.1±0.6%, n=25; 7.6±1.0%, n=20, p<0.05) were smaller in sh-NL1 expressing neurons (Fig. 2c–f), consistent with reduced NMDAR content in individual spines. Both NMDAR-uEPSCs and Ca^{2+} influx were restored or increased beyond control levels by coexpression of sh-NL1 and hNL1 (Fig. 2c–f, NMDAR-uEPSCs: 18.1±2.4 pA, n=21, p>0.05 vs. control; $\Delta G/G_{sat}$: 15.3±1.4%, n=21, p<0.05). Similarly, larger NMDAR-uEPSCs and Ca^{2+} transients were measured from spines of cells transfected with hNL1 alone (Fig. 2c–f; NMDAR-uEPSCs: 26.0±2.7 pA, n=21, p<0.05; $\Delta G/G_{sat}$: 19.9±1.7%, n=21, p<0.05). This positive correlation between NL1 levels and NMDAR-mediated synaptic signals suggests that NL1 facilitates incorporation or retention of NMDARs in the postsynaptic terminal, consistent with previous studies [31, 33, 38].

The peak amplitude of uEPSCs measured at −60 mV was not modulated by NL1 levels, but its decay was slowed in hNL1-transfected neurons (Fig. 2c). To determine if this prolongation resulted from alterations of AMPAR properties or if it represented an unusual contribution of NMDAR currents at resting potentials, we repeated recordings in the presence of the NMDAR antagonist CPP (10 μM). CPP application abolished the spine and dendrite Ca^{2+} signals as well as the slow component of uEPSC, confirming that all were due to NMDAR activation (Fig. 2d).

Parallel analyses were carried out in NL1−/− mice (Fig. 3), in which NMDAR/AMPAR current ratios have been previously reported to be reduced in hippocampal CA1 pyramidal neurons, amygdala principal neurons, and striatal medium spiny neurons [19, 24, 39]. Consistent with these reports, we found that glutamate uncaging evoked AMPAR-uEPSCs measured from individual spines of layer 2/3 pyramidal neurons were not different between NL1−/− and NL1+/+ littermate mice, whereas NMDAR-uEPSCs were significantly smaller in NL1−/−mice (Fig. 3a,d; NL1+/+ and NL1−/−: AMPAR-uEPSCs: 10.7±1.3 pA, n=24, 8.6 ± 1.2 pA, n=25, p>0.05, NMDAR-uEPSCs: 9.9±1.2 pA, n=24, 4.0±0.8 pA, n=25, p<0.05). NMDAR-mediated spine Ca^{2+} influx was also reduced (Fig. 3b; NL1+/+ and NL1−/−: $\Delta G/G_{sat}$: 8.8±1.1%, n=24, 5.2±0.6 pA, n=25, p<0.05). Furthermore, introducing sh-NL1 into NL1−/− KO neurons had no effect on NMDAR-uEPSCs and Ca^{2+} influx, indicating that, as expected for an NL1-dependent phenomenon, sh-NL1-mediated effects were occluded by constitutive loss of NL1 (Fig. 3a–d; NL1−/−+sh-NL1: AMPAR-uEPSCs, NMDAR-uEPSCs, and spine $\Delta G/G_{sat}$: 11.0±1.3 pA, 5.2±0.6 pA, and 4.9±0.5%, n=20, p>0.05 for each vs.

NL1$^{-/-}$). Thus, the effects of NL1 loss on synaptic NMDARs are similar in the global knock-out and RNAi-induced sparse knock-down, indicating that the level of NL1 in each cell intrinsically regulates NMDAR-signaling but not excitatory synapse number.

Neuroligin-1 levels modulate glutamate-induced spinogenesis

Overexpression of NL1 in dissociated neuronal cultures influences synapse number in an activity-dependent manner[19], suggesting that NL1 regulates the selection of synapses after initial synapse formation. To determine if NL1 also regulates initial synapse formation, we utilized a glutamate uncaging protocol that triggers the rapid and *de novo* formation of a spine and the establishment of a new synapse (Fig. 4a)[35]. This process requires activation of dendritic NMDA receptors, which are perturbed by changes in NL1 expression (see below).

In wild-type animals, sparse knock-down of NL1 in layer 2/3 pyramidal neurons by RNA interference lowered, whereas overexpression of NL1 increased, the success rate of new spine generation (Fig. 4b,c). The magnitude of the effects depended on the frequency of stimulation such that NL1 overexpression enhanced the low probability of spinogenesis seen with low-frequency stimuli whereas down-regulation of NL1 decreased the high success rate triggered by higher frequency stimuli. In contrast, the same class of neurons in NL1 KO mice displayed normal activity-dependent spinogenesis. Furthermore, the normal synaptogenetic potential of neurons in NL1 KO mice occurs despite a ~50% reduction in dendritic NMDAR currents (Fig. 4d,e; NL1$^{+/+}$ and NL1$^{-/-}$: NMDAR-uEPSCs: 10.0±2.1 pA, n=15, 5.9±0.9 pA, n=15, p<0.05), which was not different from that seen in shNL1 transfected neurons in WT animals (Fig. 4d,e; 4.7±0.9 pA, n=16, p>0.05). Thus, sparse but not global manipulations of NL1 modulate the threshold of activity-dependent spinogenesis, likely explaining the parallel observations in synapse and spine number at later developmental stages.

Excitatory synapse number is regulated by relative levels of Neuroligin-1

The findings that synapse number and structure are altered in neurons with NL1 knock-down but not in neurons with NL1 KO may be explained by a transcellular competitive mechanism[40, 41]. In this model, a cell expressing higher levels of NL1 relative to its neighbors has an advantage in forming synapses. For example, each cortical neuron might compete in NL1-dependent manner with surrounding neurons to establish proper connectivity with a limited number of presynaptic boutons. If correct, this mechanism explains why manipulations that eliminate NL1 from all neurons fail to recapitulate the perturbations seen in genetically mosaic tissue.

To test this model, we performed co-culture experiments in which NL1$^{+/+}$ and NL1$^{-/-}$ neurons were mixed. We used *in utero* electroporation to transfect EGFP into layer 2/3 pyramidal neurons of NL1 KO mice. Cultures of cortical neurons were prepared by mixing, at specific ratios, cells dissociated from these manipulated NL1 KO mice and age-matched wild-type mice (Fig. 5a). Consistent with the competition hypothesis, neurons in pure cultures of NL1$^{-/-}$ or NL1$^{+/+}$ cells had similar spine densities (Fig. 5c; NL1$^{+/+}$ and NL1$^{-/-}$: 1.03±0.03 spines/μm, 37 fields of view, 1.01±0.05 spines/μm, 21 fields of view, p>0.05). However, when NL1$^{-/-}$ cells were mixed 1:1 with NL1$^{+/+}$ neurons, spine density in the NL1$^{-/-}$ cells was reduced (Fig. 5c; 0.58±0.05 spines/μm, 16 fields of view, p<0.05). Spine density was further reduced when the ratio of NL1$^{-/-}$ to NL1$^{+/+}$ cells was reduced to 1:5 (Fig. 5c; 0.39±0.04 spines/μm, 18 fields of view, p<0.05). Thus, the spine density of NL1$^{-/-}$ cortical layer 2/3 pyramidal neurons in culture depends on the fraction of co-cultured neurons that express NL1, indicating that transcellular interactions determine synapse number. These results are obtained without use of RNA-interference, demonstrating context-dependent defects in synapse numbers in neurons with constitutive genetic loss of NL1.

Levels of endogenous neuroligin-1 expression vary across cortical neurons

To understand whether neuron-to-neuron variability in NL1 expression *in vivo* could support the competitive model presented above, we measured mRNA levels by fluorescence *in situ* hybridization (ISH) across cortical neurons (Fig. 6). NL1 mRNA was detected throughout all cortical layers without layer-specific expression (Fig. 6a,b). To determine the degree of variation of NL1 expression in cortical layer 2/3, we performed two-color fluorescence ISH of NL1 and GAPDH (Fig. 6c). Levels of endogenous NL1 mRNA expression show large cell-to-cell variation compared to GAPDH (Fig. 6c,d), resulting in a larger coefficient of variation (GAPDH and NL1: 26.1±1.6%, n=10 fields and 37.7±4.3%, n=10, p<0.05).

Gradients of NL1 levels across cortical neurons regulate spine number

To directly test *in vivo* if transcellular gradients of NL1 expression level regulate synapse number, we examined a variety of conditions where NL1 expression is higher or lower in a cell few relative to neighbors (Supplementary Fig. 4). First, we examined whether spine density is regulated in a dose-dependent manner by NL1. We took advantage of a specific sh-NL1, sh-NL1#9, which partially reduced NL1 levels (Fig. 1a). When transfected into neurons of WT animals, sh-NL1#9 reduced spine density only slightly (0.7±0.03 spines/μm, 27 dendrites, p<0.05 vs. wildtype). In contrast a second very efficient shRNA, sh-NL1#4, greatly reduced spine density (0.4±0.04 spines/μm, 15 dendrites, p<0.05 vs. wildtype).

Second, if the magnitude of transcellular gradients in NL1 levels determines the density of excitatory synapses, then spine density in a sparse subset of neurons that over-express NL1 in $NL1^{-/-}$ mice should be higher than in neurons that over-express NL1 in wild-type mice. Indeed, spine density in hNL1 transfected neurons in $NL1^{-/-}$ mice was very high (Fig. 7a–c; 1.9±0.1 spines/μm, 10 neurons, 17 dendrites, p<0.05 vs. hNL1 in WT, 1.4±0.1 spines/μm, 11 neurons, 22 dendrites). Increased density of spines was accompanied by increased mEPSC frequency, indicating that more functional synapses had been made (Fig. 7a–c; hNL1 in $NL1^{-/-}$, 3.67±0.35 Hz, n=8, p<0.05 vs. hNL1 in WT, 2.19±0.43 Hz, n=6).

Furthermore, across many manipulations the magnitude of changes in spine density and mEPSC frequency induced by manipulations of NL1 depend on the NL1 content of neighboring neurons. The effects of NL1 knock-down are reduced in the $NL1^{+/-}$ hemizygote mice and completely absent in $NL1^{-/-}$ mice (Fig. 7e,f; sh-NL1 in WT, $NL1^{+/-}$, and $NL1^{-/-}$: percent change in spine density: −42±6%, −30±3%, −1±5% compared to the matched background; percent change in mEPSC frequency: −58±12%, n=8, −27±12%, n=8, 1±11%, n=9). Conversely, the effects of overexpression of NL1 are more dramatic when NL1 levels are reduced in neighboring cells (Fig. 7e,f; hNL1 in WT, $NL1^{+/-}$, and $NL1^{-/-}$: percent change in spine density: 47±5%, 68±6%, 102±9% compared to the matched background; percent change in mEPSC frequency: 79±43%, n=6, 155±30%, n=10, 187±28%, n=8). The changes in spine density and synapse number seen with perturbation of NL1 levels are not due to variability in these parameters across animals, as they are observed when WT neurons, sh-NL1 expressing, and hNL1 overexpressing neurons in the same slice are compared (Fig. 7f,g) (spine density: sh-NL1, 0.53±0.06 spines/μm, n=12 neurons/22 dendrites; control, 1.06±0.05, n=9/15; hNL1, 1.40±0.05, n=8/19. mEPSC frequency: sh-NL1, 0.37 ± 0.17 Hz, n=5; control, 1.47±0.18, n=7; hNL1, 2.18±0.30, n=5 neurons. mEPSC amplitude: sh-NL1, 9.3±0.8 pA; control, 10.8±0.5; hNL1, 9.4±0.4 pA). Thus, spine density and mEPSC frequency in each cell are determined not by the cell's absolute level of NL1 but the difference in its levels of NL1 relative to neighboring neurons.

DISCUSSION

The functions of NL1 *in vivo* in regulating synaptogenesis and the number of excitatory synapses per neuron have been controversial, with some studies concluding direct functions of NL1 in both processes and other studies proposing a later function of NL1 in activity-dependent synapse validation[19, 27, 42]. To resolve some of these controversies, we examined, in a variety of genetic contexts, synaptic and cellular properties of cortical layer 2/3 pyramidal neurons whose levels of NL1 had been altered. Furthermore, we compared the effects of sparse vs. global manipulations to determine if synapses are sensitive to the absolute levels of NL1 in an individual cell or to relative differences in NL1 compared to neighboring neurons.

Our data reveal that the defects in cellular development depend on the context in which NL1 is perturbed. Loss of NL1 in all cells, and in only a subset of cortical layer 2/3 neuron, equally alter the level of extra-synaptic and synaptic NMDARs, consistent with previous results [19, 24–26]. However, when NL1 levels are decreased or increased in one cell relative to its neighbors, additional functions of NL1 in regulating activity-dependent spinogenesis and synapse number are revealed. Thus, neurons that have relatively high levels of NL1 grow new spines more readily, leading to increased spine density and functional synapse number. In contrast, neurons with relatively low levels of NL1 are deficient in the same parameters.

Regulation of synapse number, spine density, and synaptogenesis by transcellular gradients in NL1

NLs have been proposed to act in the initial stages of synapse formation to promote synaptogenesis[27]. This hypothesis was supported by the demonstration that the number of synapses or spine density decreased with reduction of NL and increased with enhanced expression[19, 28–34]. Recently, it was alternatively proposed that NLs function in synapse specification and validation such that synapses initially form in an NL-independent manner but their stabilization or maintenance require validation by NLs[19]. However, each hypothesis has been tested in different systems and supported differentially by *in vitro* and *in vivo* data. Furthermore, often the effects of NL1 on synapse number were seen following RNA-interference mediated knock-down, which is susceptible to difficult to exclude off-target effects[43].

To directly examine the role of NL1 *in vivo* in synapse formation, we manipulated NL1 expression levels in either a subset of neurons or in all neurons and examined the effects on *de novo* activity-dependent spinogenesis and mature synapse number. All of our analyses are performed in cortical layer 2/3 pyramidal neurons. We conclude that relative differences in NL1 across neurons determine the potential for initial synapse formation, which likely underlies the changes in excitatory synapse density observed in more mature neurons. Importantly, we demonstrated that the effects of RNA-interference against NL1 are due specifically to loss of NL1 as they were prevented by co-expression of human NL1, recapitulated by several shRNA sequences, and, most importantly, not seen when the shRNA was expressed in NL1 KO mice. This last control should be considered the gold-standard for off-target effects in RNA-interference based studies.

Thus, *in vivo* analyses indicate that NL1 levels in one cell that are high relative to its neighbors put it at advantage in the process of synapse formation, resulting in higher density of excitatory synapses. These results were confirmed *in vitro* since cultured GFP-labeled NL1$^{-/-}$ layer 2/3 pyramidal neurons only display defects in spine density when mixed with NL$^{+/+}$ neurons. The intercellular or intersynapse processes that determine spine number and growth may include competition for binding to presynaptic neurexins and displacement by

NL1 of other neurexin binding partners such as LRRTMs (Leucine-rich repeat transmembrane neuronal proteins)[44, 45].

Regulation of individual synapses by NL1

Our study also reveals that the absolute and relative levels of NL1 regulate individual synapses. Loss of NL1 in all contexts decreases NMDAR-evoked currents and calcium influx by ~50% and spine morphology is altered by sparse manipulation of NL1 (Supplementary Fig. 1), consistent with previous reports[19, 29]. These morphological changes are likely to have a functional impact, as spines with a large head and long neck trap signaling molecules for longer periods [46, 47]. Indeed we found altered Ca^{2+} signaling in spines and dendrites of neurons with altered NL1 expression as well as perturbations of diffusion of activated fluorophores across the neck. This impacts the temporal and spatial profiles of signaling pathways involved in synaptic formation, maturation, and plasticity. For example, PKA is anchored in the dendrite at rest, but when activated the catalytic subunit moves into the spine and facilitates induction of long-term potentiation[48], a process that may be hampered by narrow and long spine necks.

Conclusion

This study resolves previous conflicts in the literature by demonstrating that the effects of NL1 on synaptogenesis and synapse number are highly context dependent. Combined *in vitro* and *in vivo* results demonstrate that defects in synaptogenesis and synapse number are revealed in NL1 lacking neurons if neighboring neurons express NL1. Similarly, the degree of perturbation of synapse number is graded depending on the relative differences in NL1 across neurons.

EXPERIMENTAL PROCEDURES

Plasmids

Mouse neuroligin-1 tagged with GFP on its C-terminal end[49] was a gift of Dr. Nils Brose in Max-Planck-Institute, Germany. Human NL1 cDNA was purchased from OriGene (Cat #. SC127261). Four different target sequences for shRNA directed against mouse NL1 (sh-NL1 #1~4) were designed using the online utilities of the Whitehead Institute for Biomedical Research. 19~21 bp coding, loop, and reverse complementary sequence nucleotides were synthesized (Integrated DNA Technologies) and ligated into pGUR, a vector that produces shRNA under an U6 promoter and EGFP under a CMV promoter[50]. Four additional sh-NL1 constructs (sh-NL1 #6~9) from Sigma were tested (Cat #. NM_138666). Western blot analysis showed that sh-NL1 #4 and #7 efficiently reduced NL1 levels. The nucleotide sequences for sh-NL1 #4 and #7 are:

sh-NL#4: GGGGGAAGGGTTGAAGTTTGTTTCAAGAGAACAAACTTCAACCCTTCCCCC CTTTTTG and AATTCAAAAAGGGGGGAAGGGTTGAAGTTTGTTCTCTTGAAACAAACTTCA A CCCTTCCCCC

sh-NL1 #7: GGGCAGACCTTCACTCGAACTTTCTCGAGAAAGTTCGAGTGAAGGTCTGCC CCTTTTTG and AATTCAAAAAGGGGCAGACCTTCACTCGAACTTTCTCGAGAAAGTTCGAGT G AAGGTCTGCCC

Cell culture, transfection and viral infection

For the experiments to validate the efficiency of sh-NL1, 1×10^5 HEK293 cells were plated and 1 µg of NL1-GFP and 4 µg of sh-NL1. DNA was transfected using a Calcium phosphate transfection kit (Cat # 44-0052, Invitrogen). Cells were harvested two days later and the lysate was used for the Western blotting.

Organotypic hippocampal slice cultures were prepared from 7~8 day old Spraque Dawley rats[51]. The brain was taken out and immediately placed in chilled dissection media. Transverse hippocampal slices were chopped with 400~500 µm thickness and 4~6 slices were placed in a sterile culture plate insert (Millicell-CM, Millipore) in 6-well plates containing prewarmed media. DNA was biolistically transfected with a Helios Gene Gun (Biorad) 2 days after culturing. Bullets were made with 60 µg of DNA or, for the rescue experiments, 40 µg each of sh-NL1 and hNL1. For the viral infection experiments, dissociated hippocampal cultures were prepared from 1 day old rats. 1×10^5 neurons were plated in poly-d-lysine coated 24-well plates. Two days later, 3 infectious units of viruses per cell were added to the culture media and cells were harvested at 7~8 days after infection. Lentiviruses expressing sh-NL1 and control virus were purchased from Sigma (MISSION Lentiviral Transduction Particles, for sh-NL1 #7: Cat # TRCN0000032021, for control: Cat #: SHC001V). Antibodies for Western blots were: Neuroligin-1, 2, and 3 from Synaptic Systems (Gottingen, Germany); GAPDH from Cell Signaling Technology.

In utero electroporation

All procedures for animal surgery and maintenance were performed following protocols approved by the Harvard Standing Committee on Animal Care and in accordance with National Institutes of Health guidelines. To target neocortical layer 2/3 pyramidal neurons, E15.5 timed-pregnant female C57BL/6 mice (Charles River, Massachusetts, United States) were deeply anesthetized by intraperitoneal injection of 2.5% Avertin (2, 2, 2-Tribromoethanol) or 2% isoflurane. Uterine horns were carefully exposed and 1~2 µl of DNA (1 µg/µl) were injected into one lateral ventricle. To visualize the injection, 0.005% fast green was mixed with the DNA. Glass micropipettes for the injection were pulled, the tip broken to be ~50 µm in diameter, and beveled at 18° (NARISHIGE, Japan). After injection, the embryo head was held with a tweezer with round plate electrodes (0.5 mm diameter) and electric pulses were delivered five times per second (50 V, 50 ms) (CUY21 electroporator, NEPA GENE, Japan). Warm PBS was dropped onto embryos periodically to prevent drying. The uterus was placed back into the pregnant mouse, and the anterior muscle and the skin were sutured separately. Pups were housed with the dam until they were needed. For the experiments shown in Fig. 7e–g, pups *in utero* electroporated with hNL1 and tdTomato were intracranially injected at post-natal day 1 with 250 nl of ~10^9 titer lentivirus encoding shNL1 and GFP (Sigma MISSION Lentiviral Transduction Particles TRCN0000032021-CMV-tGFP), using a protocol analogous to that described previously for adeno-associated viruses[54].

In situ hybridization and image analysis

Double fluorescence *in situ* hybridization (ISH) was performed using a tyramide signal amplification method according to the manufacturer's instructions (NEL753001KT, PerkinElmer). Briefly, brains of 1 month old mice were dissected and immediately frozen in liquid nitrogen. The brains were cut into 25 µm sections with a cryostat (Leica), postfixed in 4% PFA, acetylated in 1% triethanolamine and 0.25% acetic anhydride, prehybridized, and hybridized at 65°C using the following anti-sense probes: *Nlgn1* (RP_050607_01_G08, Allen Institute for Brain Science), *Gapdh* (RP_050531_01_D11, Allen Institute for Brain Science), and *EGFP* (U55761, nt159-754). For *in vitro* transcription, NL1 cDNA was synthesized from Genscript and GAPDH cDNA was cloned out from a mouse cDNA

library. Two fluorescein-or digoxigenin-labeled riboprobes generated by an *in vitro* transcription method (Promega) were hybridized simultaneously and stained by fluorescein or Cy3 chromogens, respectively. After staining, sections were mounted with Prolong Gold antifade reagent (P36934, Invitrogen). Images were collected by fluorescence microscopy using a Nikon Eclipse 80i microscope equipped with a Nikon DS-2 digital camera. For mRNA expression analysis, images were collected by confocal laser scanning microscopy using a Zeiss LSM 510 META and processed using Image J (National Institutes of Health). Images from wild-type brain sections were taken at 40X magnification and ten cells clustered in the layer 2/3 area were randomly selected per image for analysis. To quantify the NL1 and GAPDH mRNA expression level, areas with positive *in situ* signal for each gene in the same cell were measured using Image J and the coefficient of variation for NL1 and GAPDH mRNA levels were calculated from each image. The quantitative data from ten images were compiled and analyzed.

Spine analysis

Spine head area and length were analyzed using a MATLAB program described previously[52]. For each spine, one line was drawn along the length of spine (major axis) and the other line was drawn to cross the first line at the middle of spine head where the fluorescent intensity is maximum (minor axis). Head area was calculated by counting the number of pixels inside the area where fluorescent intensity remains to 30% of the maximal value. Spine length was designated as the distance to the point along the major axis where fluorescence dropped to 30% of the peak.

Acute slice preparation

C57BL/6 mice (17~25 days old) were deeply anesthetized with isoflurane and decapitated. The brain was rapidly removed and placed in chilled choline-based cutting solution containing (in mM) 25 $NaHCO_3$, 1.25 NaH_2PO_4, 2.5 KCl, 7 $MgCl_2$, 25 glucose, 1 CaCl2, 110 choline chloride, 11.6 ascorbic acid, and 3.1 pyruvic acid. Coronal sections of the brain were cut at 300μm thickness using a Leica VT1000S vibratome (Leica Instruments, Nussloch, Germany) in cold cutting solution. Slices were transferred to ACSF containing (in mM) 127 NaCl, 2.5 KCl, 25 $NaHCO_3$, 1.25 NaH_2PO_4, 2 $CaCl_2$, 1 $MgCl_2$, and 25 glucose. Both cutting and ACSF solution were saturated with 95% O_2 and 5% CO_2 (pH 7.4). The slices were incubated at room temperature for at least 1 hour before recording.

Electrophysiology

A slice was transferred to a recording chamber perfused with ACSF. All voltage-clamp recordings were performed at room temperature, and current-clamp recordings at 32°C. For voltage-clamp recordings, the electrode was filled with an internal solution containing (in mM) 120 $CsMeSO_3$, 8 NaCl, 15 $CsCl_2$, 10 TEA·Cl, 10 HEPES, 2 QX-314, 4 MgATP, and 0.3 Na_2GTP (pH 7.3). The pipette resistance was 3–4 MΩ. For current clamping recording, the patch electrode was filled with 120 $KMeSO_4$, 5 KCl, 5 HEPES, 4 MgATP, and 0.3 Na_2GTP, and 10 phosphocreatine (pH 7.3). Patch pipettes were pulled with a micropipette puller (P-97, Sutter instrument). Whole-cell recordings were made from cortical layer 2/3 pyramidal neurons. For Ca^{2+} imaging experiments, at least 10 minutes were allowed to pass after breaking the cell membrane before searching for a spine for analysis. For mEPSC recordings, cells were clamped at −60 mV in the presence of 10 μM CPP and 10 μM bicuculine. To measure AMPAR- and NMDAR-uEPSCs, uEPSCs were measured first at −60 mV and then at +40 mV. Glutamate uncaging-evoked EPSCs were measured in the presence of 10 μM d-serine, 1 μM TTX, 1 μM ω-conotoxin-MVIIC, 20 μM nimodipine, and 3 μM mibefradil. All recordings were made with a MultiClamp 700A (Axon Instruments Inc., Union City, CA, USA).

Two-photon microscope and uncaging

Uncaging of MNI-glutamate and Ca^{2+} imaging was achieved using a custom-built microscope combining two-photon laser-scanning microscopy (2PLSM) and two-photon laser photoactivation (2PLP) as previously described[53]. Two mode-locked Ti:Sapphire lasers (Chameleon, Coherent, Santa Clara, CA) were used for imaging and uncaging at wavelengths of 840 nm and 720 nm, respectively. Alexa-594 (20 μM) and Fluo-5F (300 μM) were loaded in the cell through the recording patch pipette. 5 mM MNI-glutamate was perfused in the recirculating bath and a 500 μs duration laser pulse at 720 nm was delivered to the target spot to release glutamate. Ca^{2+} transients shown in Figure 2, 3, and 4 are plotted in units of $\Delta G/G_{sat}$ which was calculated by dividing $\Delta G/R$ by G_{sat}/R. G_{sat}/R was measured in a 1:1 mixture of 1 M $CaCl_2$ and internal solution, which saturates the Ca^{2+} indicator. At least five consecutive responses (AMPAR-, NMDAR-uEPSCs, and Ca^{2+} transients) were averaged from each spine. To deliver a constant stimulus to each spine, laser power was set to bleach red fluorescence in each spine head by ~40% [36].

Animals

B6;129 NL1$^{+/-}$ (heterozygous) mice were kindly provided from Dr. Nils Brose lab (Max-Planck-Institute, Germany). Genotyping was accomplished by PCR of genomic DNA from the mouse tail. The primers used for genotyping are:

428, GAGCGCGCGCGGCGGAGTTGTTGAC;

430, GTGAGCTGAATCTTATGGTTAGATGGG;

561, CGGTCAACAAACCTACTCAGAATCAGG. All data shown in Figure 1, 3 and 7 were obtained from NL1$^{-/-}$ and littermate control NL1$^{+/+}$ resulting from heterozygous mating. Both male and female mice were used for the experiments.

Statistics

The Kolmogorov-Smirnov test was used to determine significance of differences in spine morphology. To determine significant differences of success rate of spinogenesis, Fisher's exact test was used. For all other experiments, statistical significance was judged using a student t-test (two-sided) or one way analysis of variance followed by Newman-Keuls multiple comparison *post hoc* tests. $P < 0.05$ was judged as significant.

Supplementary Material

Refer to Web version on PubMed Central for supplementary material.

Acknowledgments

References

1. Katz LC, Shatz CJ. Synaptic activity and the construction of cortical circuits. Science. 1996; 274:1133–8. [PubMed: 8895456]

2. Sanes JR, Yamagata M. Many paths to synaptic specificity. Annu Rev Cell Dev Biol. 2009; 25:161–95. [PubMed: 19575668]

3. Huberman AD, Feller MB, Chapman B. Mechanisms underlying development of visual maps and receptive fields. Annu Rev Neurosci. 2008; 31:479–509. [PubMed: 18558864]

4. Moody WJ, Bosma MM. Ion channel development, spontaneous activity, and activity-dependent development in nerve and muscle cells. Physiol Rev. 2005; 85:883–941. [PubMed: 15987798]

5. Grutzendler J, Kasthuri N, Gan WB. Long-term dendritic spine stability in the adult cortex. Nature. 2002; 420:812–6. [PubMed: 12490949]

6. Hofer SB, Mrsic-Flogel TD, Bonhoeffer T, Hubener M. Experience leaves a lasting structural trace in cortical circuits. Nature. 2009; 457:313–7. [PubMed: 19005470]

7. Trachtenberg JT, et al. Long-term in vivo imaging of experience-dependent synaptic plasticity in adult cortex. Nature. 2002; 420:788–94. [PubMed: 12490942]

8. Alvarez VA, Sabatini BL. Anatomical and physiological plasticity of dendritic spines. Annu Rev Neurosci. 2007; 30:79–97. [PubMed: 17280523]

9. Dalva MB, McClelland AC, Kayser MS. Cell adhesion molecules: signalling functions at the synapse. Nat Rev Neurosci. 2007; 8:206–20. [PubMed: 17299456]

10. Scheiffele P. Cell-cell signaling during synapse formation in the CNS. Annu Rev Neurosci. 2003; 26:485–508. [PubMed: 12626697]

11. Sudhof TC. Neuroligins and neurexins link synaptic function to cognitive disease. Nature. 2008; 455:903–11. [PubMed: 18923512]

12. Contractor A, et al. Trans-synaptic Eph receptor-ephrin signaling in hippocampal mossy fiber LTP. Science. 2002; 296:1864–9. [PubMed: 12052960]

13. Yamagata M, Sanes JR, Weiner JA. Synaptic adhesion molecules. Curr Opin Cell Biol. 2003; 15:621–32. [PubMed: 14519398]

14. Song JY, Ichtchenko K, Sudhof TC, Brose N. Neuroligin 1 is a postsynaptic cell-adhesion molecule of excitatory synapses. Proc Natl Acad Sci U S A. 1999; 96:1100–5. [PubMed: 9927700]

15. Varoqueaux F, et al. Neuroligins determine synapse maturation and function. Neuron. 2006; 51:741–54. [PubMed: 16982420]

16. Ichtchenko K, et al. Neuroligin 1: a splice site-specific ligand for beta-neurexins. Cell. 1995; 81:435–43. [PubMed: 7736595]

17. Ichtchenko K, Nguyen T, Sudhof TC. Structures, alternative splicing, and neurexin binding of multiple neuroligins. J Biol Chem. 1996; 271:2676–82. [PubMed: 8576240]

18. Jamain S, et al. Reduced social interaction and ultrasonic communication in a mouse model of monogenic heritable autism. Proc Natl Acad Sci U S A. 2008; 105:1710–5. [PubMed: 18227507]

19. Chubykin AA, et al. Activity-dependent validation of excitatory versus inhibitory synapses by neuroligin-1 versus neuroligin-2. Neuron. 2007; 54:919–31. [PubMed: 17582332]

20. Poulopoulos A, et al. Neuroligin 2 drives postsynaptic assembly at perisomatic inhibitory synapses through gephyrin and collybistin. Neuron. 2009; 63:628–42. [PubMed: 19755106]

21. Durand CM, et al. Mutations in the gene encoding the synaptic scaffolding protein SHANK3 are associated with autism spectrum disorders. Nat Genet. 2007; 39:25–7. [PubMed: 17173049]

22. Feng J, et al. High frequency of neurexin 1beta signal peptide structural variants in patients with autism. Neurosci Lett. 2006; 409:10–3. [PubMed: 17034946]

23. Jamain S, et al. Mutations of the X-linked genes encoding neuroligins NLGN3 and NLGN4 are associated with autism. Nat Genet. 2003; 34:27–9. [PubMed: 12669065]

24. Blundell J, et al. Neuroligin-1 deletion results in impaired spatial memory and increased repetitive behavior. J Neurosci. 2010; 30:2115–29. [PubMed: 20147539]

25. Kim J, et al. Neuroligin-1 is required for normal expression of LTP and associative fear memory in the amygdala of adult animals. Proc Natl Acad Sci U S A. 2008; 105:9087–92. [PubMed: 18579781]

26. Soler-Llavina GJ, Fuccillo MV, Ko J, Sudhof TC, Malenka RC. The neurexin ligands, neuroligins and leucine-rich repeat transmembrane proteins, perform convergent and divergent synaptic functions in vivo. Proc Natl Acad Sci U S A. 2011; 108:16502–9. [PubMed: 21953696]

27. Scheiffele P, Fan J, Choih J, Fetter R, Serafini T. Neuroligin expressed in nonneuronal cells triggers presynaptic development in contacting axons. Cell. 2000; 101:657–69. [PubMed: 10892652]

28. Boucard AA, Chubykin AA, Comoletti D, Taylor P, Sudhof TC. A splice code for trans-synaptic cell adhesion mediated by binding of neuroligin 1 to alpha- and beta-neurexins. Neuron. 2005; 48:229–36. [PubMed: 16242404]

29. Chih B, Engelman H, Scheiffele P. Control of excitatory and inhibitory synapse formation by neuroligins. Science. 2005; 307:1324–8. [PubMed: 15681343]

30. Dean C, et al. Neurexin mediates the assembly of presynaptic terminals. Nat Neurosci. 2003; 6:708–16. [PubMed: 12796785]

31. Graf ER, Zhang X, Jin SX, Linhoff MW, Craig AM. Neurexins induce differentiation of GABA and glutamate postsynaptic specializations via neuroligins. Cell. 2004; 119:1013–26. [PubMed: 15620359]

32. Levinson JN, El-Husseini A. Building excitatory and inhibitory synapses: balancing neuroligin partnerships. Neuron. 2005; 48:171–4. [PubMed: 16242398]

33. Nam CI, Chen L. Postsynaptic assembly induced by neurexin-neuroligin interaction and neurotransmitter. Proc Natl Acad Sci U S A. 2005; 102:6137–42. [PubMed: 15837930]

34. Prange O, Wong TP, Gerrow K, Wang YT, El-Husseini A. A balance between excitatory and inhibitory synapses is controlled by PSD-95 and neuroligin. Proc Natl Acad Sci U S A. 2004; 101:13915–20. [PubMed: 15358863]

35. Kwon HB, Sabatini BL. Glutamate induces de novo growth of functional spines in developing cortex. Nature. 2011; 474:100–4. [PubMed: 21552280]

36. Bloodgood BL, Sabatini BL. Nonlinear regulation of unitary synaptic signals by CaV(2.3) voltage-sensitive calcium channels located in dendritic spines. Neuron. 2007; 53:249–60. [PubMed: 17224406]

37. Sabatini BL, Oertner TG, Svoboda K. The life cycle of Ca(2+) ions in dendritic spines. Neuron. 2002; 33:439–52. [PubMed: 11832230]

38. Barrow SL, et al. Neuroligin1: a cell adhesion molecule that recruits PSD-95 and NMDA receptors by distinct mechanisms during synaptogenesis. Neural Dev. 2009; 4:17. [PubMed: 19450252]

39. Jung SY, et al. Input-specific synaptic plasticity in the amygdala is regulated by neuroligin-1 via postsynaptic NMDA receptors. Proc Natl Acad Sci U S A. 2010; 107:4710–5. [PubMed: 20176955]

40. Buffelli M, et al. Genetic evidence that relative synaptic efficacy biases the outcome of synaptic competition. Nature. 2003; 424:430–4. [PubMed: 12879071]

41. McClelland AC, Hruska M, Coenen AJ, Henkemeyer M, Dalva MB. Trans-synaptic EphB2-ephrin-B3 interaction regulates excitatory synapse density by inhibition of postsynaptic MAPK signaling. Proc Natl Acad Sci U S A. 2010; 107:8830–5. [PubMed: 20410461]

42. Chubykin AA, et al. Dissection of synapse induction by neuroligins: effect of a neuroligin mutation associated with autism. J Biol Chem. 2005; 280:22365–74. [PubMed: 15797875]

43. Alvarez VA, Ridenour DA, Sabatini BL. Retraction of synapses and dendritic spines induced by off-target effects of RNA interference. J Neurosci. 2006; 26:7820–5. [PubMed: 16870727]

44. de Wit J, et al. LRRTM2 interacts with Neurexin1 and regulates excitatory synapse formation. Neuron. 2009; 64:799–806. [PubMed: 20064388]

45. Ko J, Fuccillo MV, Malenka RC, Sudhof TC. LRRTM2 functions as a neurexin ligand in promoting excitatory synapse formation. Neuron. 2009; 64:791–8. [PubMed: 20064387]

46. Santamaria F, Wils S, De Schutter E, Augustine GJ. Anomalous diffusion in Purkinje cell dendrites caused by spines. Neuron. 2006; 52:635–48. [PubMed: 17114048]

47. Svoboda K, Tank DW, Denk W. Direct measurement of coupling between dendritic spines and shafts. Science. 1996; 272:716–9. [PubMed: 8614831]

48. Zhong H, et al. Subcellular dynamics of type II PKA in neurons. Neuron. 2009; 62:363–74. [PubMed: 19447092]

49. Dresbach T, Neeb A, Meyer G, Gundelfinger ED, Brose N. Synaptic targeting of neuroligin is independent of neurexin and SAP90/PSD95 binding. Mol Cell Neurosci. 2004; 27:227–35. [PubMed: 15519238]

50. Tavazoie SF, Alvarez VA, Ridenour DA, Kwiatkowski DJ, Sabatini BL. Regulation of neuronal morphology and function by the tumor suppressors Tsc1 and Tsc2. Nat Neurosci. 2005; 8:1727–34. [PubMed: 16286931]

51. Stoppini L, Buchs PA, Muller D. A simple method for organotypic cultures of nervous tissue. J Neurosci Methods. 1991; 37:173–82. [PubMed: 1715499]

52. Sturgill JF, Steiner P, Czervionke BL, Sabatini BL. Distinct domains within PSD-95 mediate synaptic incorporation, stabilization, and activity-dependent trafficking. J Neurosci. 2009; 29:12845–54. [PubMed: 19828799]

53. Carter AG, Sabatini BL. State-dependent calcium signaling in dendritic spines of striatal medium spiny neurons. Neuron. 2004; 44:483–93. [PubMed: 15504328]

54. Kozorovitskiy Y, Saunders A, Johnson CA, Lowell BB, Sabatini BL. Nature. 2012; 485:646–50. [PubMed: 22660328]
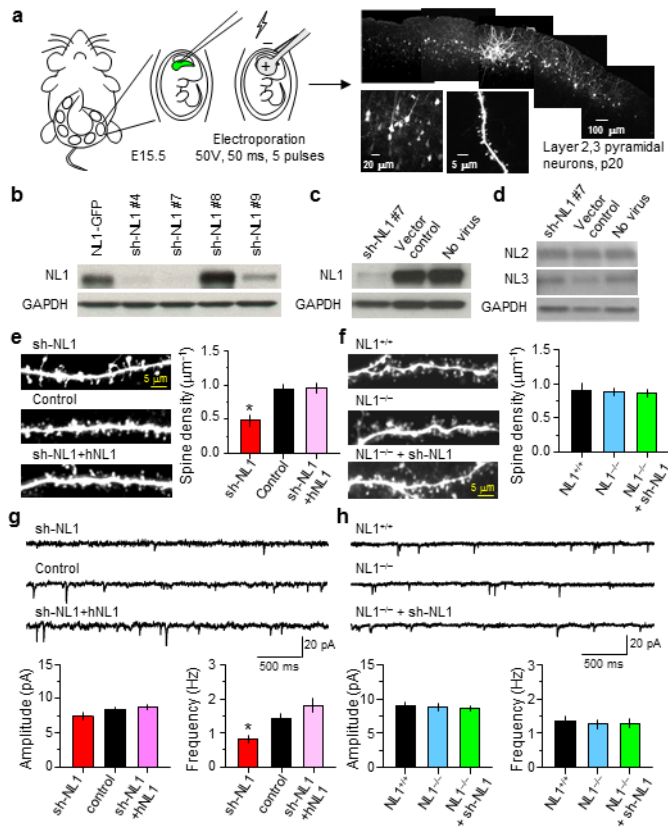
Figure 1.

Sparse knock-down of NL1 but not NL1 global knockout reduces synapse number and spine density in cortical layer 2/3 pyramidal neurons

(a) *left,* Schematic of the *in utero* electroporation method used to transfect neocortical layer 2/3 pyramidal neurons *in vivo. right,* Low and high magnification images of an acute slice showing EGFP expression in layer 2/3 pyramidal neurons.

(b) Western blot analysis of knock-down efficiency in shNL1 and NL1-GFP transfected HEK293T cells.

(c–d) Western blot analysis of endogenous NL1-3 expression in dissociated cortical cultures transduced with lentivirus encoding sh-NL1 #7 or lentivirus carrying a control vector compared to that in uninfected controls.

(e) Examples and summary of spine density in layer 2/3 pyramidal neurons in acute brain slices expressing EGFP (control), sh-NL1#7 (sh-NL1), or sh-NL1 and hNL1.

(f) Examples and summary of spine density in acute brain slices of NL1$^{+/+}$, NL1$^{-/-}$, and NL1$^{-/-}$ neurons transfected with sh-NL1.

(g–h) Representative mEPSCs (*top*) and their average amplitude and frequency (*bottom*) for neurons of each indicated genotype. Error bars: s.e.m. *: p<0.05 vs. control.
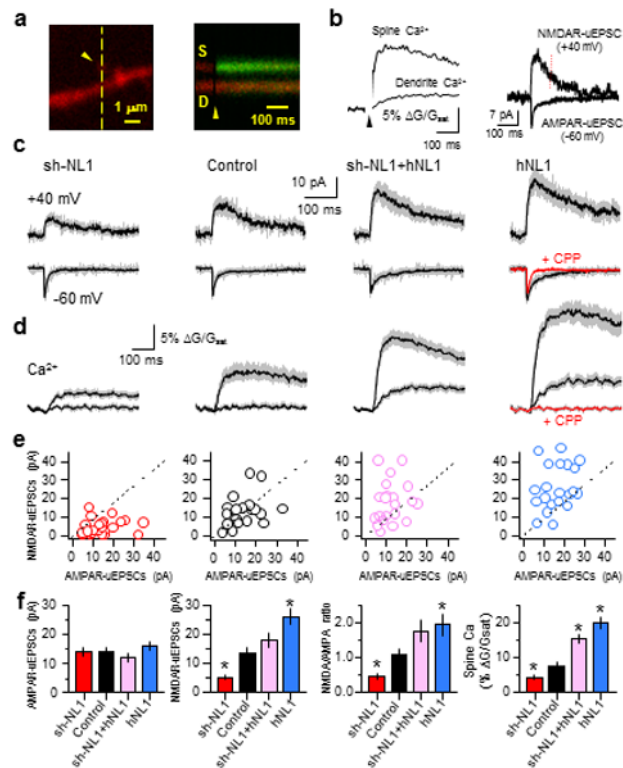
Figure 2.
Neuroligin-1 modulates NMDAR-mediated currents and Ca^{2+} signaling at individual postsynaptic terminals

(a) *left,* Image of a spine and dendrite filled with 20 μM Alexa-594 and 300 μM Fluo-5F showing the location of the glutamate uncaging spot (arrow head) and the orientation of the line scan (dashed line). *right,* Time course of fluorescent transients measured in the line scan following glutamate uncaging at the time indicated by the arrow head. Increased green fluorescence indicates Ca^{2+} entry.

(b) *left*, Quantification of the green fluorescence transient in the spine and neighboring dendrite at −60 mV. *right*, AMPAR- and NMDAR-mediated uEPSCs at −60 and +40 mV, respectively. The red dashed line (70 ms after uncaging pulse) indicates the time at which the amplitude of NMDAR-uEPSCs was measured.

(c) Average uEPSCs at −60 mV and +40 mV for neurons of the indicated genotypes and from hNL1 transfected neurons in the presence of CPP (red trace).

(d) Average Ca^{2+} transients in spines (larger traces) and dendrites (smaller traces) for neurons of the indicated genotypes −60 mV.

(e) Distributions of AMPAR- and NMDAR-uEPSCs amplitudes for each spinein each genotype.

(f) Summary of (*left* to *right*) AMPAR-uEPSC amplitude, NMDAR-uEPSC amplitude, NMDAR- to AMPAR-uEPSC amplitude ratio, and spine Ca^{2+} are shown. Error bars represent s.e.m.
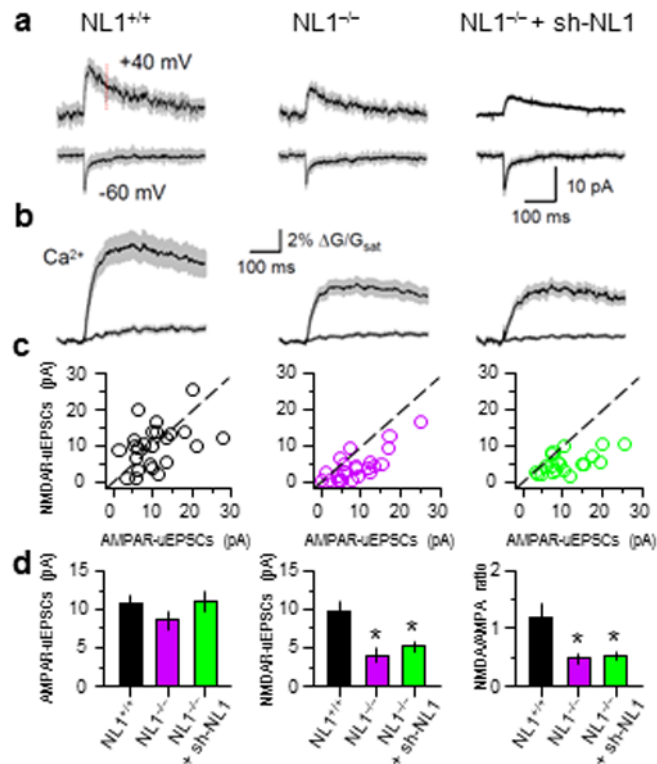
Figure 3.
Constitutive NL1 knock-out lowers NMDAR-uEPSCs and Ca^{2+} transients
(a and b) Average AMPAR- and NMDAR-uEPSCs (a) and spine and dendrite Ca^{2+}
transients at −60 mV (b) for neurons of the indicated genotypes.
(c) Relationship between AMPAR- and NMDAR-uEPSCs measured in the indicated
genotypes.
(d) Average amplitudes of AMPAR- (*left*) and NMDAR- (*middle*) uEPSCs and NMDAR/
AMPAR current ratios (*right*).
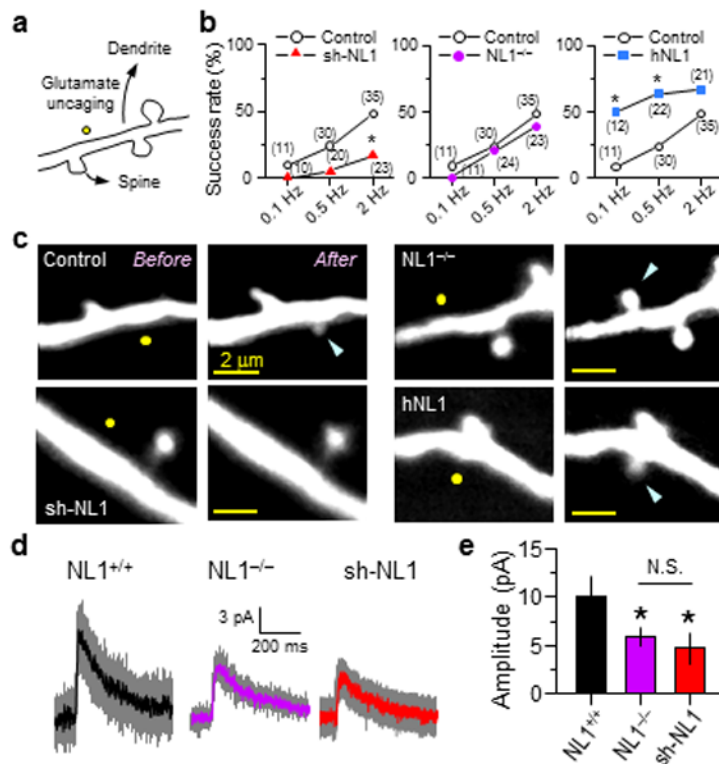
Figure 4.

NL1 regulates activity-dependent spinogenesis

(a) Schematic of glutamate-induced spinogenesis. Dendrites of EGFP-expressing cortical layer 2/3 pyramidal neurons in acute slices from P8~12 mice were visualized with 2PLSM, and glutamate (40 pulses) was released by photolysis of caged glutamate near a low-spine density section of dendrite.

(b) Success rate of *de novo* spine formation in neurons where NL1 level is reduced or increased. The numbers of attempts are shown in parentheses. *:p<0.05 vs. control.

(c) Representative images of attempted spinogenesis experiments from WT neurons transfected with EGFP, sh-NL1, or hNL1, and from an EGFP-transfected NL1$^{-/-}$ neuron. Yellow circles and blue arrows indicate uncaging positions and, when applicable, nascent spines, respectively.

(d–e) Average dendritic NMDAR uEPSCs (d) and amplitudes (e) recorded at +40 mV in the presence of NBQX from P9-11 neurons of the indicated genotypes. Glutamate was released 0.5 μm from the dendritic shaft.
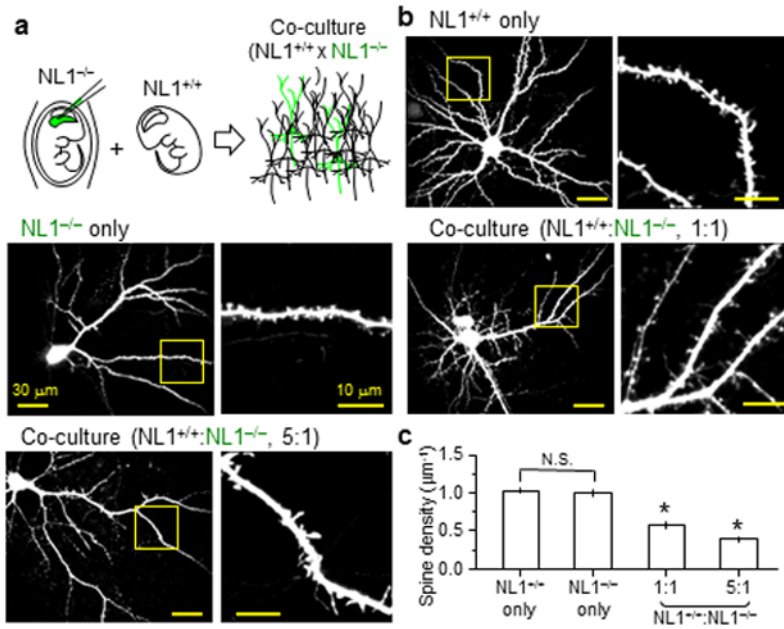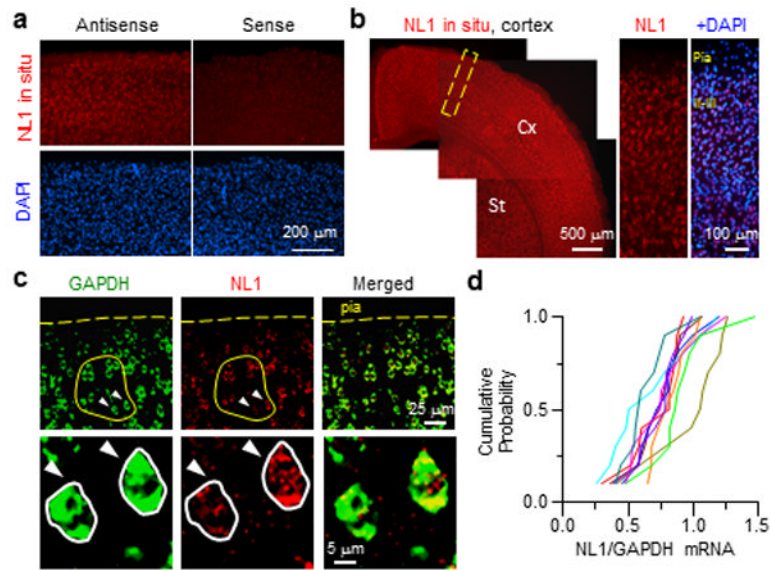
Figure 5.
Spine density of NL1$^{-/-}$ neurons *in vitro* is affected by presence of neighboring NL1$^{+/+}$ neurons

(a) Schematic of the co-culture experiment. NL1$^{-/-}$ mice were *in utero* electroporated to label layer 2/3 pyramidal neurons with EGFP. Dissociated cortical cultures were prepared from these mice and mixed with neurons of unlabelled WT mice at varying ratios.
(b) Representative low (*left*) and high (*right*) magnification images of neurons and spiny dendrites.
(c) Average spine densities in NL$^{-/-}$ neurons mixed with NL1$^{+/+}$ neurons at different ratios.

Figure 6.
Variable NL1 mRNA in across cortical neurons

(a) Fluorescence ISH using an antisense Neuroligin-1 riboprobe (*left*) shows NL1 mRNA detection in the cortex compared to control ISH with a sense riboprobe (*right*).

(b) NL1 mRNA is expressed broadly (*left,* Cx: cortex, St: striatum). A high magnification image (*right*) of the cortex (dotted box) shows NL1 mRNA in all cortical layers.

(c) Double ISH shows GAPDH (*left*) and NL1 (*middle*) in individual layer 2/3 neurons (*top*). Representative images of neighboring neurons (arrowheads) showing differential NL1 mRNA expression in spite of relatively consistent GAPDH mRNA levels (*bottom*).

(d) Cumulative probability distribution of NL1/GAPDH ISH fluorescence ratios from 10 sets (1 per/section, 3 mice) of 10 randomly picked neighboring neurons (yellow circle in (c)).
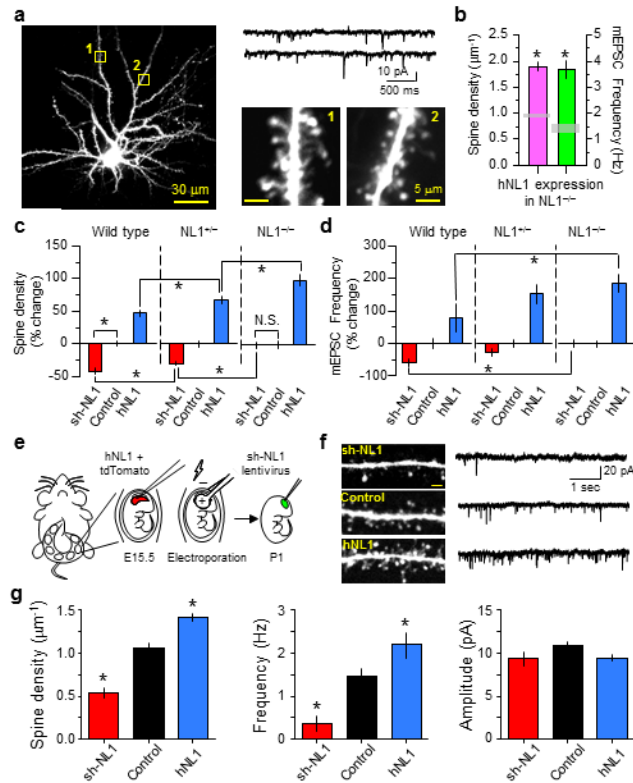
Figure 7.
Relative levels of NL1 determine spine number *in vivo* via intercellular interactions
(a) Representative hNL1-transfected neuron in an NL1$^{-/-}$ mouse showing spines and
mEPSCs.
(b) Average spine density and mEPSC frequency from hNL1-expressing neurons in NL1$^{-/-}$
mice. The gray boxes indicate the values in control neurons.
(c–d) Spine density and mEPSC frequency are differently affected by manipulating NL1
levels up (hNL1) or down (shNL1) depending the levels of NL1 in the surrounding neurons.
(e) Schematic of the experimental design. Mice were *in utero* electroporated with hNL1 +
tdTomato, followed by injection of sh-NL1 encoding lentivirus into cortex at P1.
(f) *Left*, representative images of spines from layer 2/3 pyramidal neurons infected with sh-
NL1 lentivirus (*top*), neighboring controls (*middle*), or electroporated with hNL1 +
tdTomato (*bottom*). Right, representative mEPSCs for the same 3 neuronal classes. Scale
bars, 2 μm, 2 pA and 1s.
(g) Average spine density, mEPSC frequency and amplitude in sh-NL1, control and hNL1
neurons analyzed in the same slices. Error bars: s.e.m. *: p<0.05 on *post hoc* multiple
comparison tests relative to control.